CFD Research Corporation

215 Wynn Dr. • Huntsville, AL 35805 • Tel: (256) 726-4800 • FAX: (256) 726-4806 • info@cfdrc.com

LES SOFTWARE FOR THE DESIGN OF LOW EMISSION COMBUSTION SYSTEMS FOR VISION 21 PLANTS

Quarterly Technical Progress Report for

January 2001 – March 2001

by

Steve Cannon
Virgil Adumitroaie
Keith McDaniel
Cliff Smith

May 2001 **CFDRC Report No. 8321/2**

Contract No.: DE-FC26-00NT40975

submitted to

AAD Document Control, M/S 921-107
National Energy Technology Center
U.S. Department of Energy
P.O. Box 10940
Pittsburgh, PA 15236

Technical Monitor: Dr. Kanwal Mahajan
Contract Monitor: Ms. Crystal Sharp

DISCLAIMER

ABSTRACT

Further development of a Large Eddy Simulation (LES) code for the design of advanced gaseous combustion systems is described in this second quarterly report. CFD Research Corporation (CFDRC) is developing the LES module within the parallel, unstructured solver included in the commercial CFD-ACE+ software. CFDRC has implemented and tested Smagorinsky and localized dynamic subgrid turbulence models on a 2.1 million cell DOE-NETL combustor case and a 400,000 cell nonreacting backstep case. Both cases showed good agreement between predicted and experimental results. The large DOE-NETL case results provided better agreement with the measured oscillation frequency than previous attempts because massive parallel computing (on a cluster of 24 pcs) allowed the entire computational domain, including the swirler vanes and fuel spokes, to be modeled. Subgrid chemistry models, including the conditional moment closure (CMC) and linear eddy model (LEM), are being tested and implemented. Reduced chemical mechanisms have been developed for emissions, ignition delay, extinction, and flame propagation using a computer automated reduction method (CARM). A 19-species natural gas mechanism, based on GRI2.11 and Miller-NO_x, was shown to predict rich NO_x emissions better than any previously published mechanisms. The ability to handle this mechanism in CFD-ACE+ was demonstrated by implementing operator splitting and a stiff ODE solver (DVODE). Efficient tabulation methods, including in situ adaptation and artificial neural nets, are being studied and will be implemented in the LES code. The LES combustion code development and testing is on schedule. Next quarter, initial results (including the DOE-NETL unstable combustor) with the CMC and LEM subgrid chemistry models will be completed and summarized.

TABLE OF CONTENTS

LIST OF FIGURES

1. INDRODUCTION

Vision 21 combustion systems will require innovative low emission designs and low development costs if Vision 21 goals are to be realized. In this three-year project, an advanced computational software tool will be developed for the design of low emission combustion systems required for Vision 21 clean energy plants. The LES software will be able to accurately simulate the highly transient nature of gaseous-fueled turbulent combustion so that innovative concepts can be assessed and developed with fewer high-cost experimental tests. During the first year, the project will include the development and implementation of improved chemistry (reduced full GRI mechanism), subgrid turbulence (localized dynamic), and subgrid combustion-turbulence interaction (Linear Eddy and Conditional Moment Closure) models into the CFD-ACE+ code. University expertise (Georgia Tech and UC Berkeley) will be utilized to help develop and implement these advanced submodels in the unstructured, parallel CFD flow solver. Efficient numerical algorithms that rely on *in situ* look-up tables or artificial neural networks will be used for the expensive subgrid chemical kinetic and mixing calculations. In the second year, the LES software will be evaluated and validated using experimental data from lab-scale and industrial test configurations, including important benchmark data from DOE-NETL. During the last year, seven industrial and academic partners will take the LES code and exercise it on problems of their choice. Final feedback and optimizations will then be implemented in the final release version of the LES software.

2. EXECUTIVE SUMMARY

Work in this second quarter (January – March 2001) has included further development and testing of the parallel LES methodology in CFD-ACE+. 3D LES of the unstable DOE-NETL combustor, including 2.1 million cells and a full geometric description of the swirl vanes and fuel spoke injectors, was demonstrated on a cluster of 24 pc's. The predicted frequency (234 Hertz) was in much better agreement with measurements (225 Hertz) than previous calculations. In addition, subgrid turbulence models (Smagorinsky and localized dynamic) have been tested on a nonreacting back-step flow, and good overall agreement was shown. The Conditional Moment Closure (CMC) and In Situ Adaptive Tabulation (ISAT) models are being implemented to describe subgrid chemistry. Development work also continued on the Artificial Neural Net approach that will include the Linear Eddy Model in CFD-ACE+. Reduced chemical mechanisms have been developed for methane and hydrogen, based on steady-state assumptions to the GRI2.11+Miller full mechanism. Their implementation in CFD-ACE+ has also been accomplished.

Next quarter, the following modeling capability will be implemented and tested:

1. conditional moment closure (CMC) for subgrid chemistry;
2. linear eddy model (LEM) for subgrid chemistry; and
3. reduced chemistry and efficient tabulation algorithms.

3. EXPERIMENTAL

No experiments were performed this quarter. All existing data, used for model validation, is described in Section 4. Results and Discussion.

4. RESULTS AND DISCUSSION

4.1 DOE-NETL Test Case (2.1 Million Cells-Detailed Injector Geometry)

Previously, a smaller 3D domain of the Richards and Janus lean-premixed (LPM) combustor experiment was modeled by starting at the swirler vane discharge and ending downstream in a short exhaust duct. This required a total pressure boundary at the swirler vane discharge to allow for mass flow rate fluctuations. During the second quarter, a more complete 3D model of the LPM combustor experiment was utilized that included the complete swirler and fuel spoke geometry. The flowfield from the inlet plenum to the exhaust duct was modeled using an unstructured mesh. The swirler was modeled using eleven 45° straight vanes in the fuel barrel. The swirler is located 6.98 centimeters downstream of the inlet plenum. The swirler ring is 1.9 centimeters in length. The vane width was modeled as 0.149 centimeters. The 8 fuel spokes are located 6.2 centimeters from the premixer exit and have a diameter of 0.31 centimeters. This left an axial spacing of 0.485 centimeters between the swirler vane exit and the fuel spokes. The fuel spokes are aligned perpendicular to the center axis of the barrel. The length of the fuel spokes are 1.12 centimeters, leaving a 0.15 centimeter radial spacing between the end of the fuel spokes and the inner diameter of the barrel. A surface cut-away view of the inlet plenum, swirler block, combustor, and refractory plug are shown in Figure 1. The surface mesh for the swirler block and spokes can be seen in Figure 2. A mesh size of 2,158,897 tetrahedral cells with the combustor comprising 1,306,049 cells was used to model the complete flowfield. The model was decomposed into 24 domains and is show in Figure 3 with grid at the z = 0.0 plane.

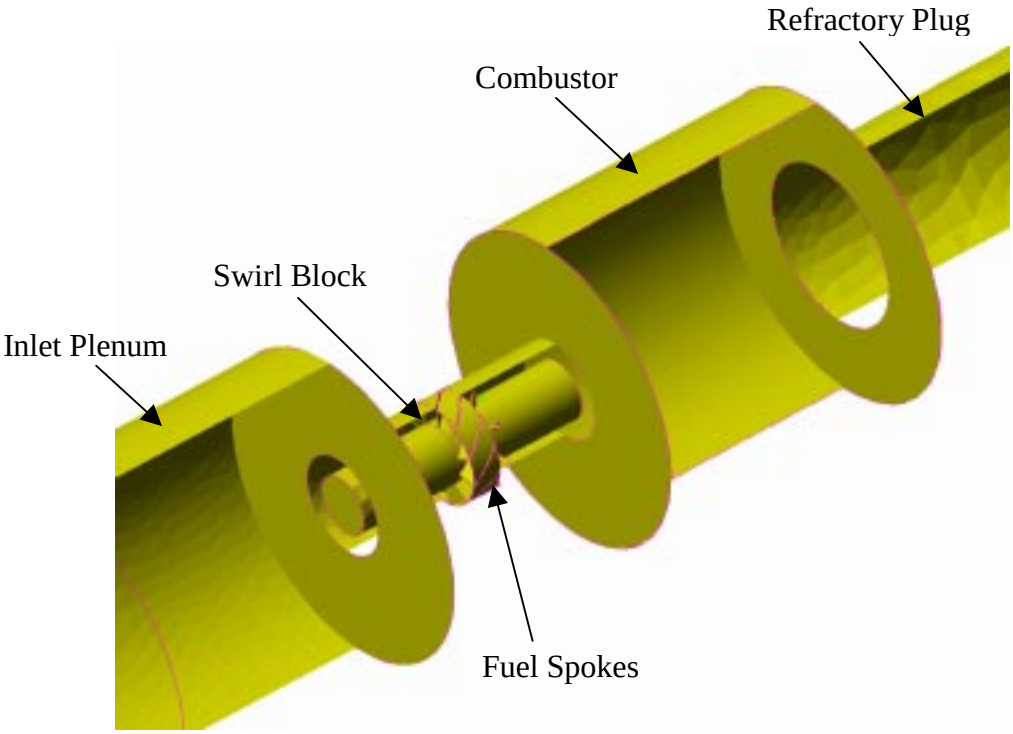

Figure 1. Surface view of Inlet Plenum, Swirler Block, Fuel Spokes, Combustor, and Refractory Plug

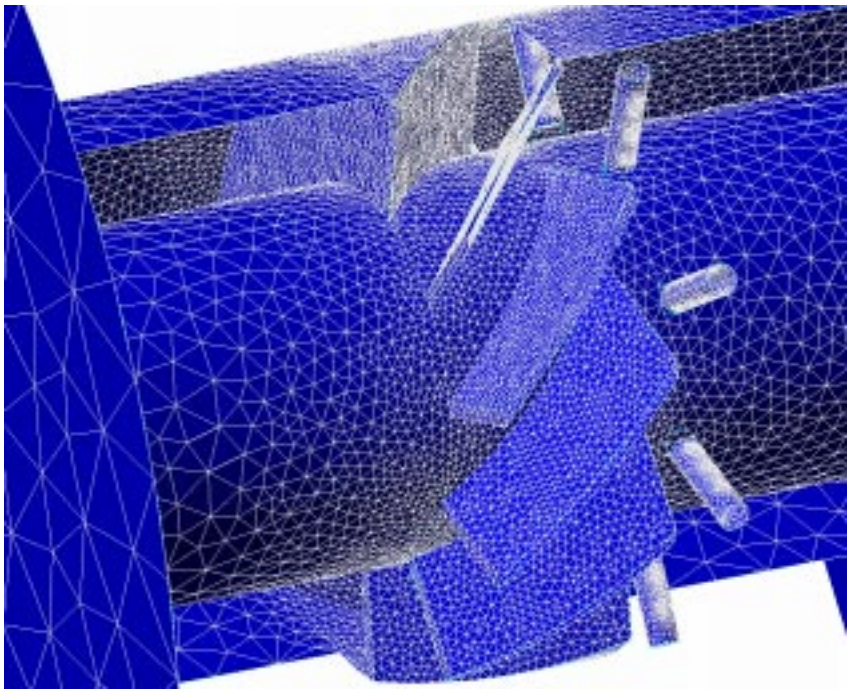

Figure 2. Surface Mesh of Swirler Vanes and Spokes

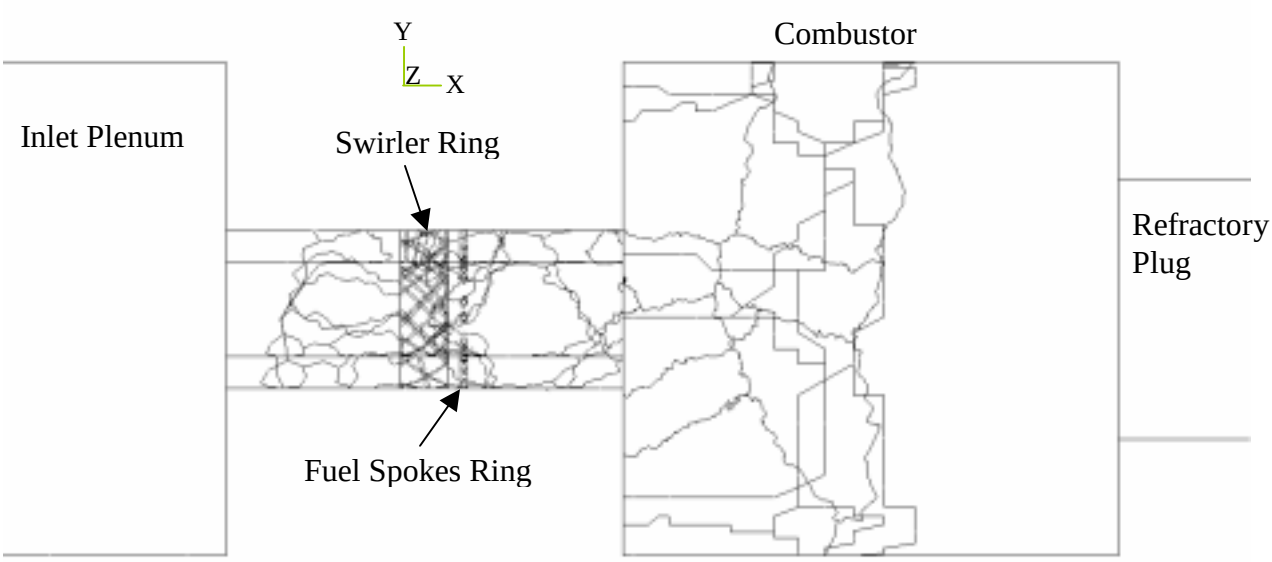

Figure 3. Decomposed Domain of Inlet, Swirler Block, Combustor, and Refractory Plug; z=0.0

By modeling the flow passage into the inlet plenum, no total pressure boundary was required for the swirler. A fixed mass flow rate of .0201 kg/s was set at the air inlet to provide 30 m/s flow through the fuel barrel. A fixed mass flow rate of .000188 kg/s was used at the fuel spoke orifices, where it is assumed that the pressure oscillations will have little effect on the fuel flow rate through the orifice. A fixed pressure boundary of 500,000 Pa was used at the outlet boundary. An isothermal wall condition is used for the combustor with T=311 K.

First a steady case was obtained with RNG k-ε and 1st order accuracy in space. This case was used as an initial condition for the transient case. Due to convergence issues, the first transient case used first order spatial and temporal resolution. Future work will resolve the convergence issues, and we plan on running second order schemes in the near future.

The steady case was also used to obtain the R parameter of the domain grid (Cannon et al, 2000). The R parameter relates the amount of separation between the local grid size, the energetic scales, and the dissipation scales. An R value less than zero implies that the filter (or grid size) is larger than the local energy containing scales, and an R greater than one implies that the resolved scales are smaller than the active viscous dissipation scales. Grid resolution should be somewhere between 0 and 1 to perform satisfactory LES. Figure 4 shows the R parameter for a y=0 plane. The R parameter is greater than one for most of the domain indicating that the grid will resolve scales that are smaller than the active viscous dissipation scales. In the region aft of the spoke ring and in the reaction zone, the R parameter is negative (approximately -0.4). Finer grid resolution is needed in those areas to resolve the energy containing scales more accurately. The Kolmogorov time scale is shown is Figure 5 for the steady calculation. It is observed here that the time scale in the combustor is always larger than 1.0e-5 seconds, which is greater than the timesteps used for the current simulation.

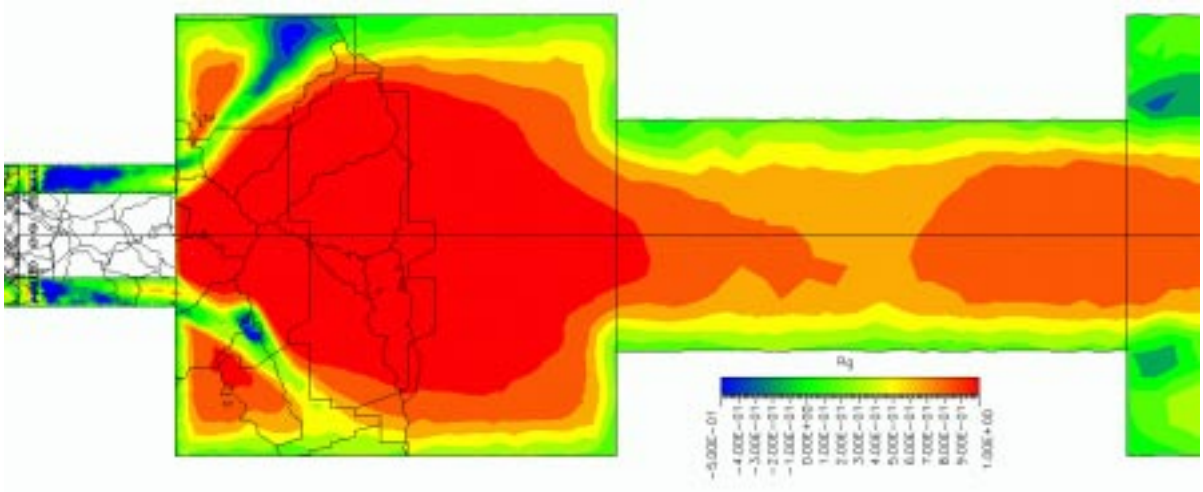

Figure 4. R parameter at y=0.0

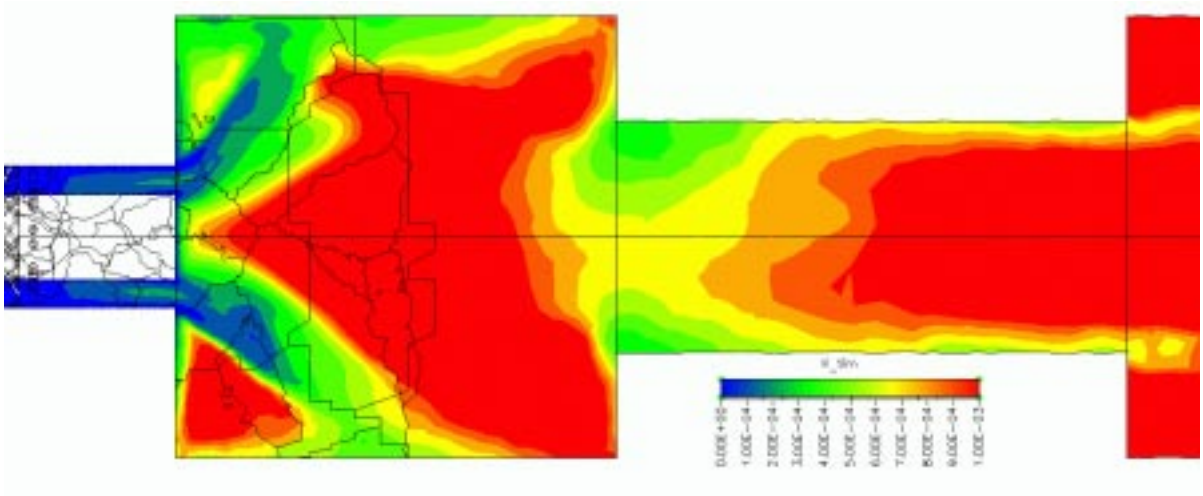

Figure 5. Kolmogorov time scale at y=0.0

The transient calculation was performed for 17 milliseconds. A timestep of 1.6e-5 seconds was used for the first 12 milliseconds, then a 2.0e-6 timestep was used to improve temporary accuracy for the remainder of the calculation. The percent pressure deviation from the average pressure in the combustor is shown in Figure 6. The maximum pressure oscillation was 1.6 percent or approximately 8 kPa. The pressure amplitude is low due to the dissipation of the 1st order calculation. A frequency of 234 Hertz in the combustor over 3 cycles was predicted. This predicted frequency was very close to the measured frequency (225 Hz) and is better than previous results without the swirler/spoke geometry (275 – 285 Hz). Our past experience has shown that temporal accuracy affects only the pressure amplitude and not the frequency of pressure oscillations (Cannon and Smith, 1998). As the time accuracy is decreased, the amplitude of the pressure oscillation is decreased. Future runs will incorporate 2nd order temporal and spatial accuracy to obtain predictions of pressure amplitude and capture combustor dynamics more accurately. The remaining figures are shown at a time level of t=0.015 seconds (the high pressure portion of the cycle).

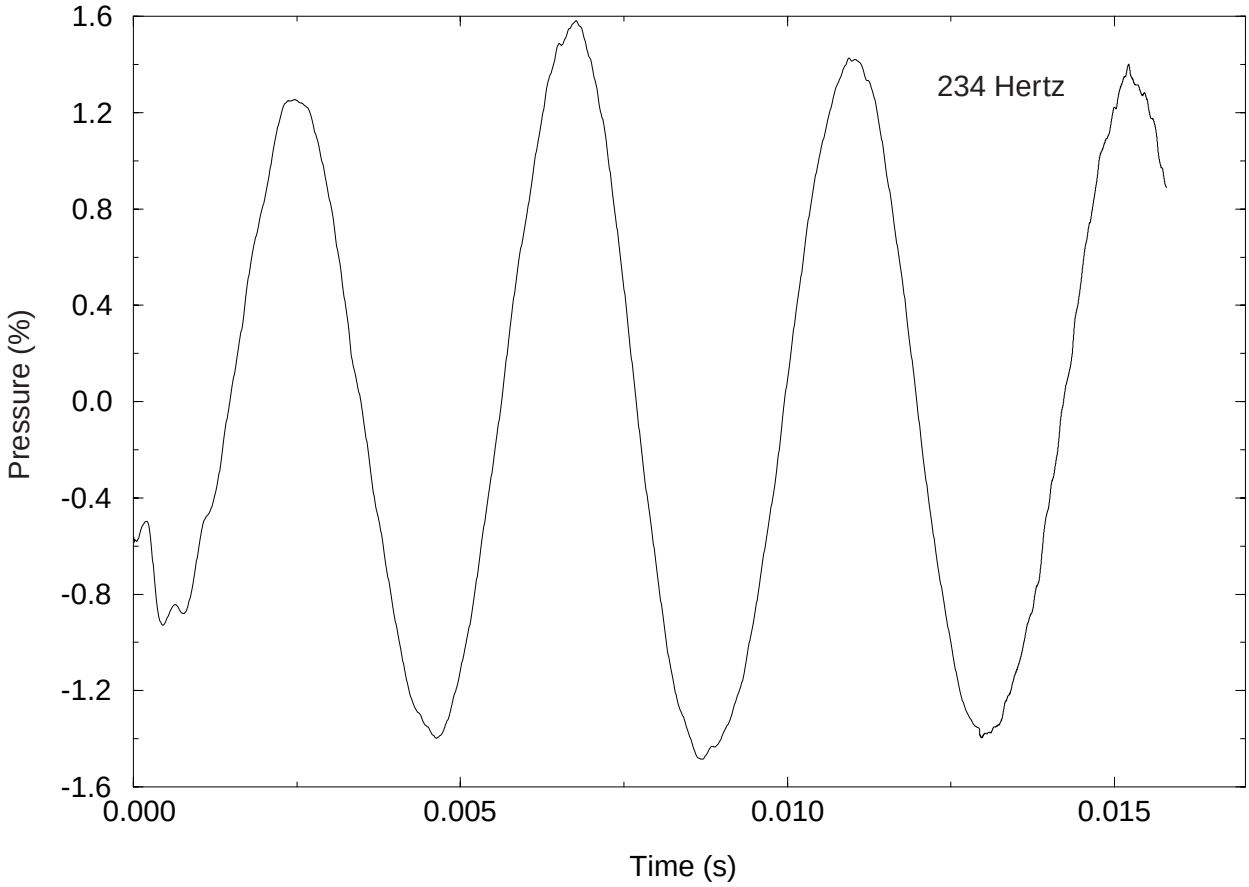

Figure 6. Percent Change in Pressure versus Time

The fuel/air equivalence ratio at the barrel dump is shown in Figure 7. The equivalence ratio is 0.85 along the inner diameter and 0.5 along the outer diameter. This radial nonuniformity was not captured in previous results and may partially explain the before-seen discrepancies in frequency between experiment and prediction. The non-uniform radial pattern of equivalence ratio is observed during the entire cycle.

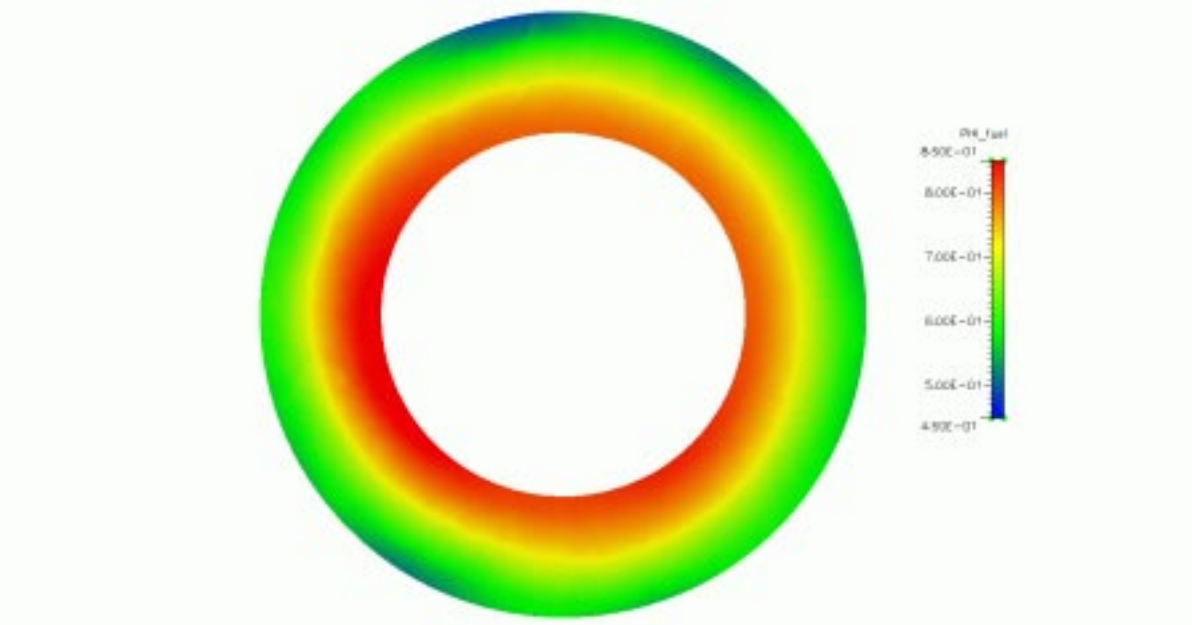

Figure 7. Fuel/air Equivalence Ratio at Barrel Dump (x=4.956, t=0.15 seconds)

The reaction rate iso-surface is plotted with superimposed temperature contours in Figure 8. This shows the structure of the flame as it is pushed outward toward the combustor wall during the high pressure portion of the cycle.

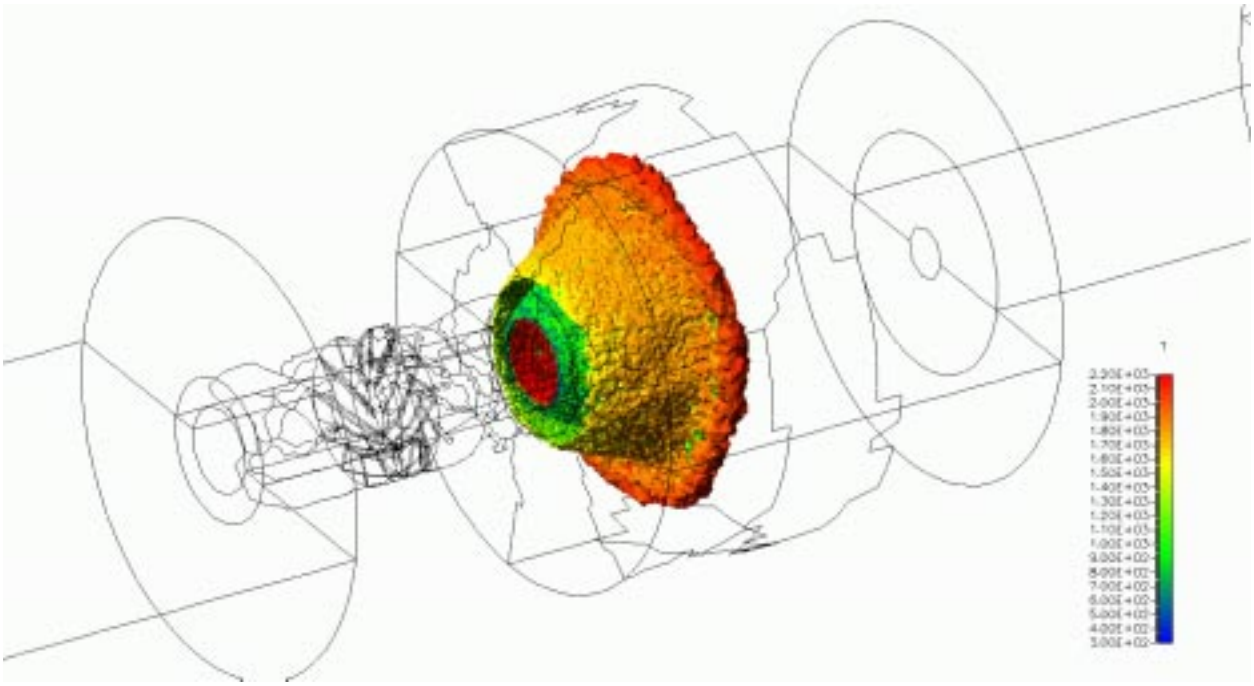

Figure 8. Reaction Rate Iso-surface with Superimposed Temperature Contours

Axial velocities are shown in several x-cuts in Figures 9 through 14, where x=-3.1, 0.0, 4.65, 6.10, and 12.86 centimeters (origin at fuel spoke). The flow through each vane passage separates from the suction side at the inlet, but re-attaches before exiting into the barrel. There are also recirculation zones in the wake of each spoke. The axial velocity is higher on the outer diameter than the inner diameter. The flow expands radially outward in the combustor finally attaching to the combustor wall. The velocity in the combustor is asymmetric in the region where the flow attaches to the wall and has been observed to oscillate about the centerline.

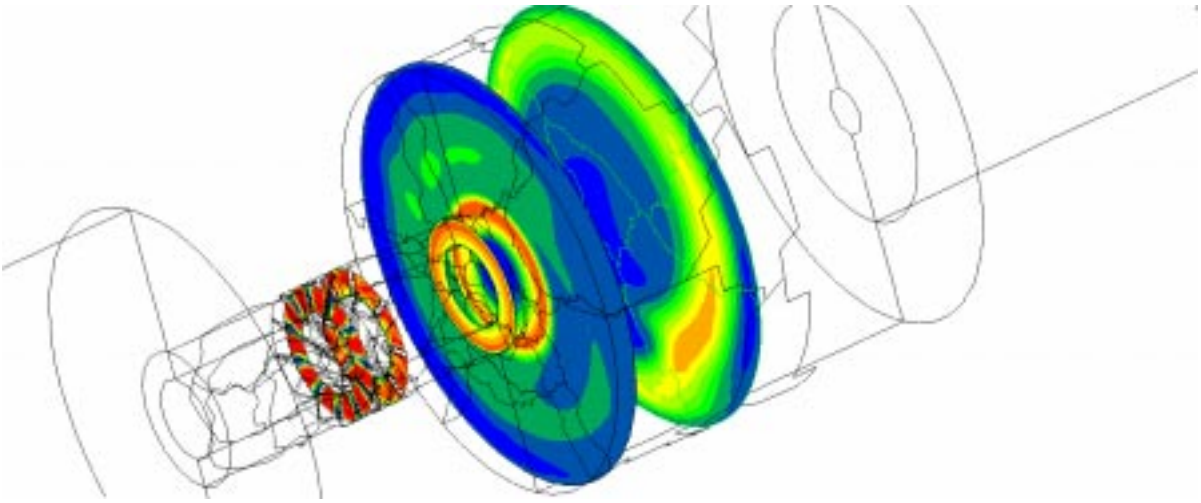

Figure 9. U Velocities Contours At x = -3.1, 0.0, 4.65, 6.10, and 12.86 centimeters

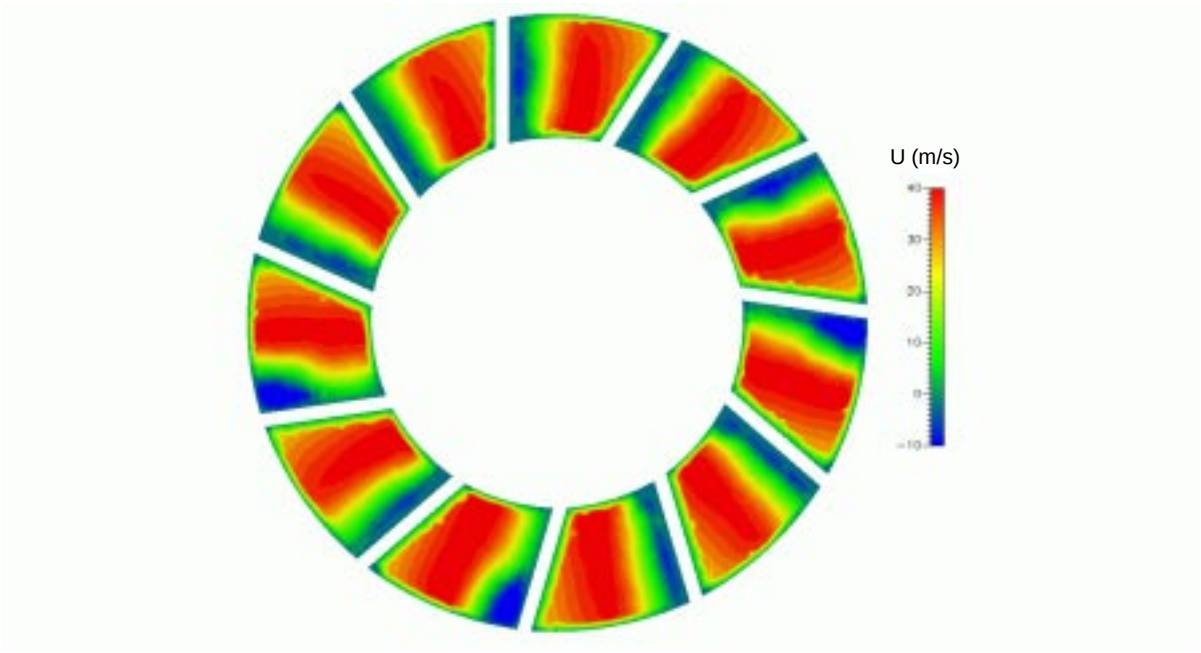

Figure 10. U Velocity Contours in Swirler Vane, x = -3.1 cm (looking downstream)

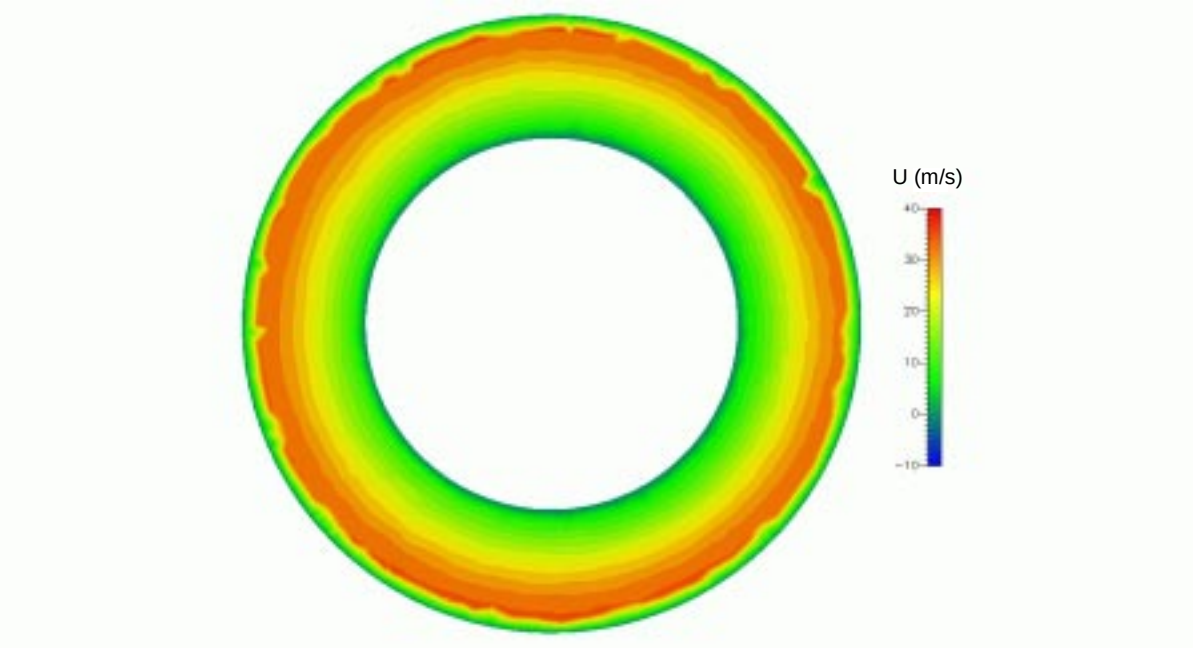

Figure 11. U Velocity Contours 1.23 cm Upstream of Spoke Ring

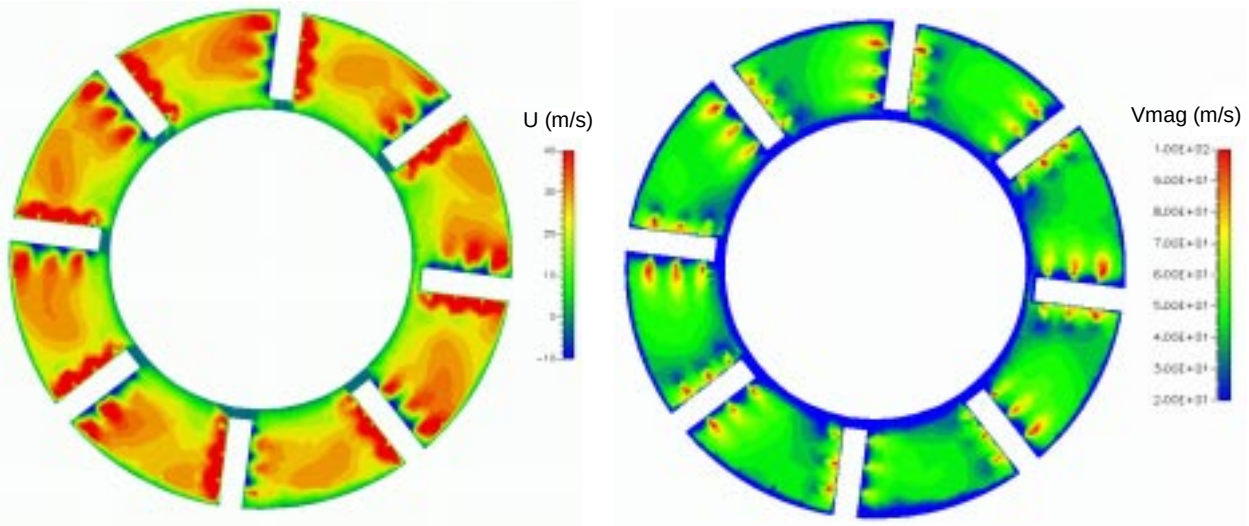

Figure 12. U Velocity and Velocity Magnitude Contours at Spoke Ring

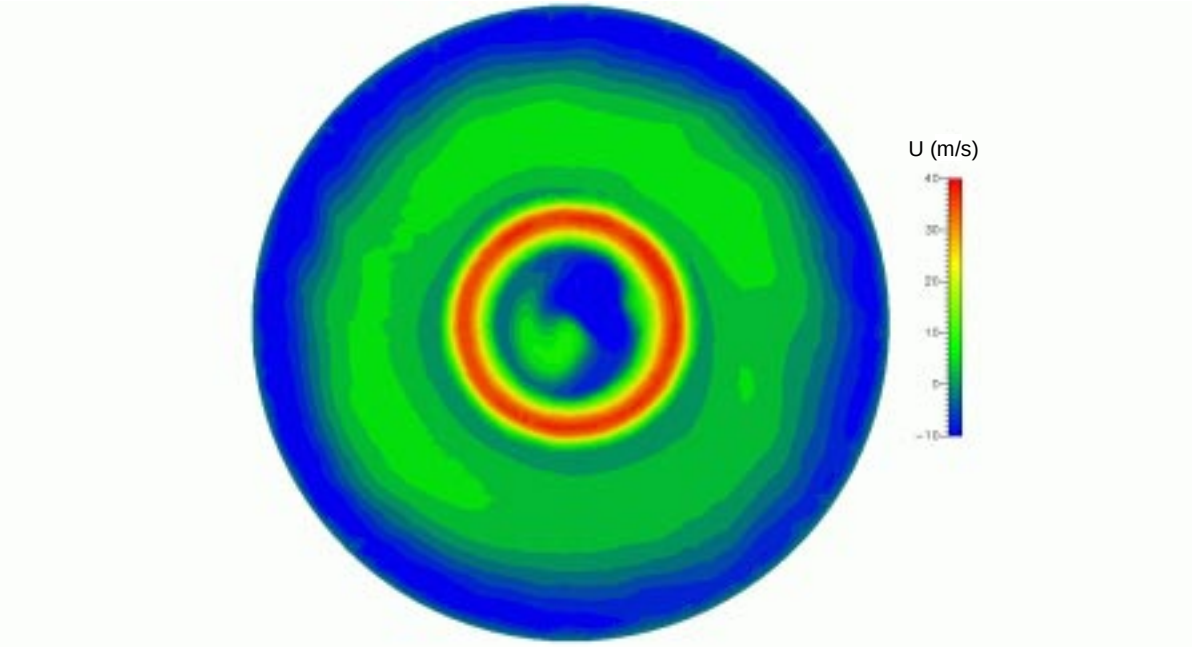

Figure 13. U Velocity Contours in Combustor, x = 6.10 cm

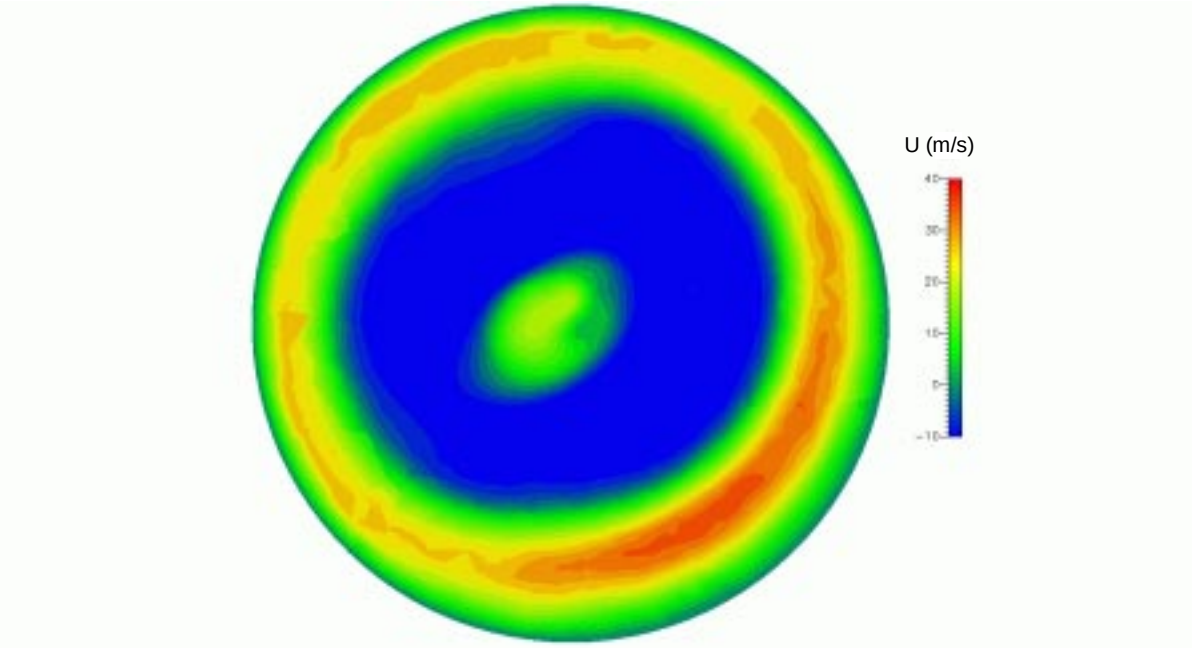

Figure 14. U Velocity Contours in Combustor, x = 12.86 cm

4.2 Localized Dynamic Subgrid-Scale Model (Ldkm) Test Case

The LDKM model development was described in the previous quarterly report. In this quarter, the LDKM model was validated in simulations of isothermal and reacting shear layers formed at a rearward facing step. LES results were compared with the experimental data taken from Pitz and Daily (1983). The experimental configuration consists of a rectilinear section followed by a smooth contraction to one half of its height, a step expansion into the test section, and a converging exit region. The computational domain is shown in Figure 15. The tests were conducted at atmospheric pressure and the mean velocity and temperature at the inlet are 13.3 m/s and 293 K. These conditions give a Reynolds number of 22,100 using the step height as the characteristic length.

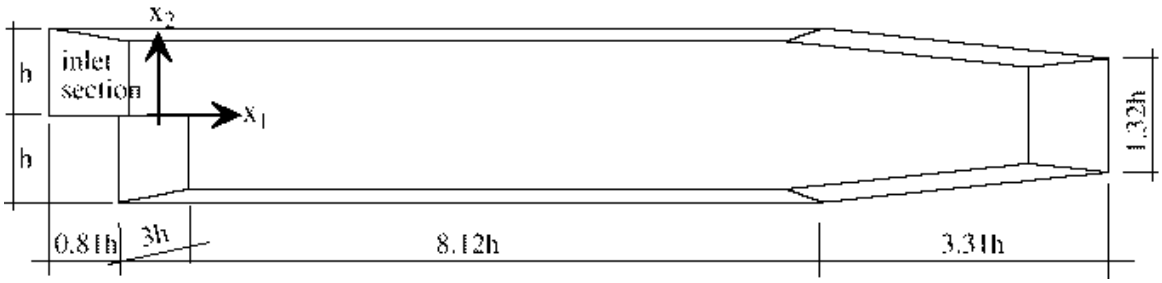

Figure 15. Computational Domain for the Backward Facing Step (Weller et al., 1998)

The computational grid consisted of 376,256 cells decomposed into 15 domains. Cells were clustered near the shear layer and towards the wall. Figure 16 shows the computational grid. The nondimensional y^+ values were between 10 and 20 along the top wall and between 1 and 8 along the bottom wall. Wall functions were used for RNG k-ε steady-state calculations and Van Driest Damping was utilized for the near-wall, Smagorinsky LES calculations. A fixed velocity and pressure were imposed at the inlet and outlet boundaries, respectively. Random fluctuations were imposed on the velocity at the inlet. Periodicity was assumed at the streamwise boundaries. Second order differencing in space (Central) and time (Crank-Nicholson) were utilized. The transient simulations were performed with a time step of 1.6e-5 seconds (maximum Courant number of 0.22) for a total of 0.504 seconds (~12 flow through times). Statistics were collected after the initial perturbation had settled out at approximately 5 flow through times. Mean and rms velocity profiles were obtained and compared to experimental data.

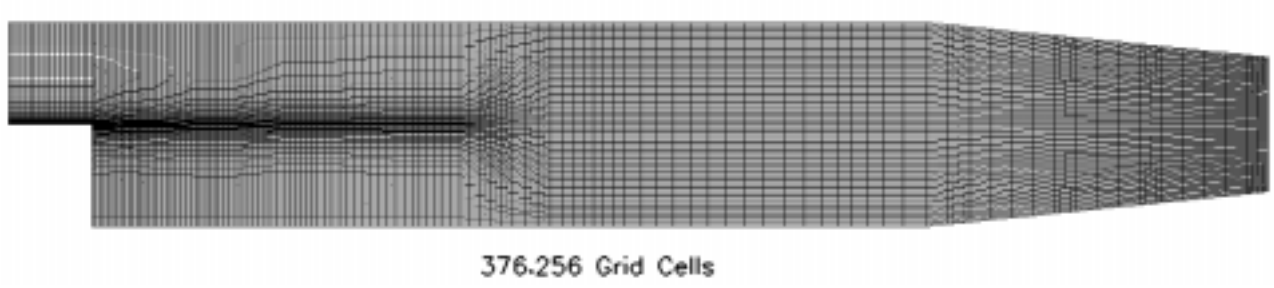

Figure 16. Grid Resolution for the Backstep Case

The inlet 13.3 m/s flow forms a shear layer downstream of the dump. Velocity and pressure oscillations occur in this shear layer as indicated in Figure 17. It is interesting to observe the high frequency oscillations in pressure that are not observed in the velocity. Low amplitude pressure oscillations (+/- 0.037%) occur, while high amplitude velocity fluctuations of +/- 6 m/s (~ 67%) are experienced. Figure 18 shows a snapshot of axial velocity at 0.496 seconds. The formed structures are irregular and 3-dimensional in nature.

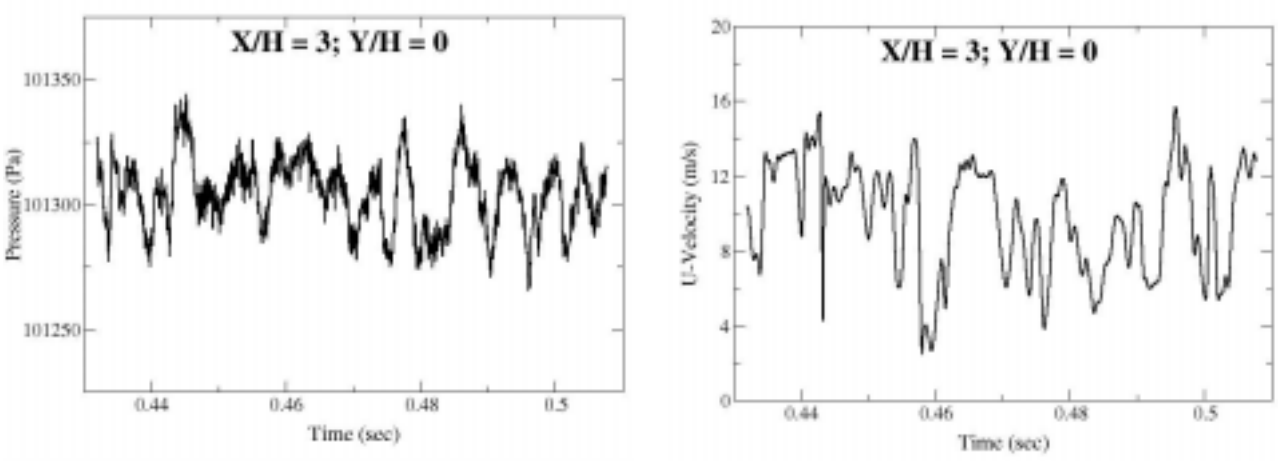

Figure 17. Predicted Pressure and Axial Velocity History at X/H=3 and Y/H=0 Using LDKM

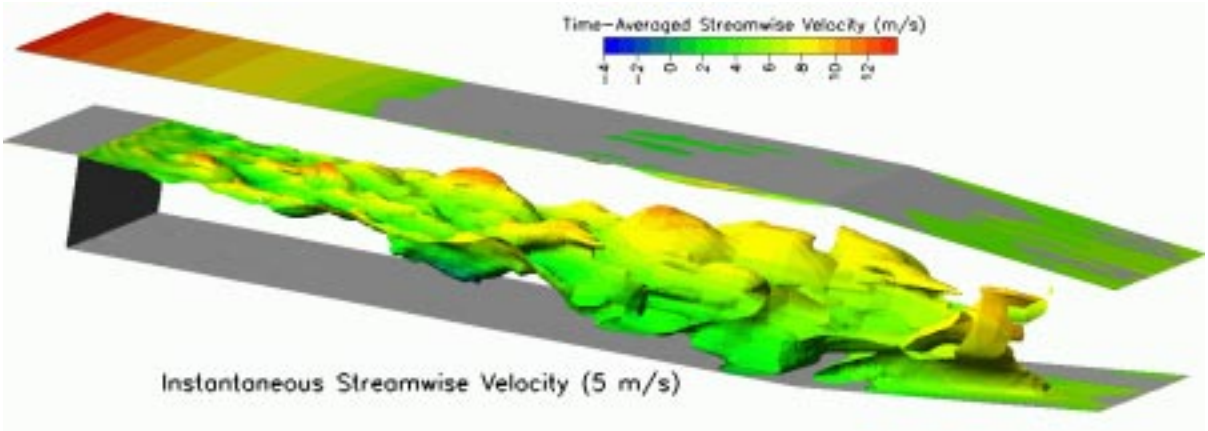

Figure 18. Predicted Instantaneous Streamwise Velocity (5 m/s) at 0.496 Seconds Using LDKM

The measured length of the recirculation zone extends 7 step heights from the dump. The LDKM predicts a reattachment length of 6.91, the Smagorinsky predicts 6.84, and the unsteady RANS (RNG k-ε) predicts 6.93. What is most interesting is that unsteady RANS does not predict any unsteady motion (i.e., unsteady RANS produces a steady-state solution), yet there is little difference between LES and unsteady RANS results for this nonreacting backstep case. Figure 19 shows comparisons between measured and predicted axial velocity profiles at various X/H locations. These results show reasonable agreement with all three models for the mean velocity profiles. All three models underpredict the spreading rate of the shear layer. At the furthest downstream location, separation occurs at the top wall using the Smagorinsky model. The RNG k-ε and LDKM models do a better job of predicting the flow at this downstream, top wall region.

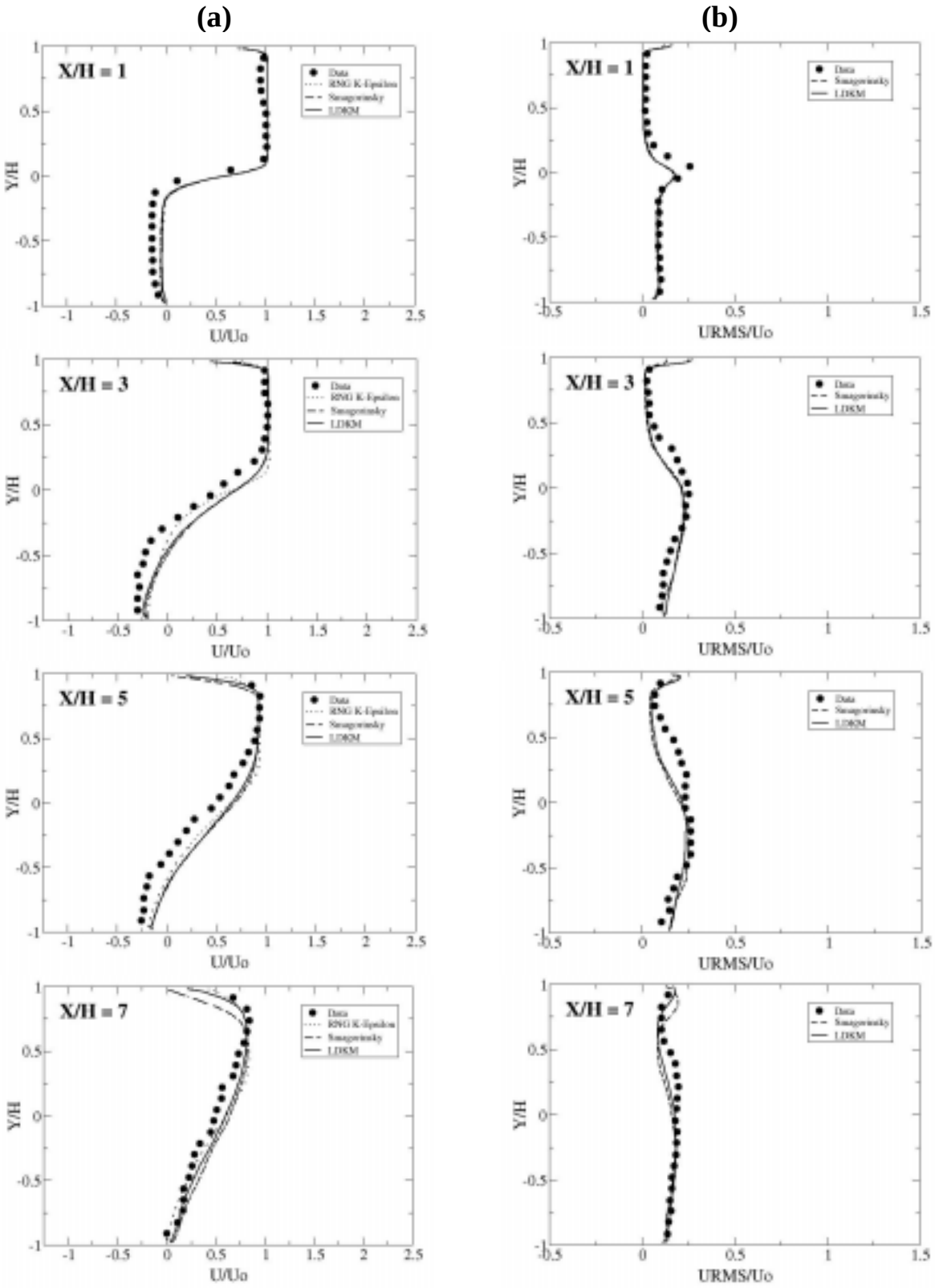

Figure 19. Comparison of Time-averaged Velocity Profiles of Streamwise (a) mean and (b) rms Velocity at Various Axial Locations

A similar LES study, performed earlier by Weller et al., (1998), showed better agreement with experimental data. They used a similar grid, with similar subgrid models and numerical accuracy. It is unclear why the LES results, in our study, are not as good as Weller et.al. Currently, fourth order pressure damping occurs in the CFD-ACE+ code to provide better convergence rates. Further work will be performed next quarter, with essentially zero pressure damping and smaller time steps, to help determine if better results can be achieved. Despite the similar mean flow field predictions between the RNG k-ε and full LES, the LES simulations will be needed to predict more complex situations that occur in swirling and reacting flows. Swirling turbulent flows introduce less isotropy and more non-equilibrium turbulence than the present back-step case. Also, the LES-predicted unsteady motions are important in capturing flame shapes and emissions that must be determined for robust combustor design. The reacting conditions are now being simulated (see Figure 20 for snapshot at 0.0096 seconds) and will be presented in the next quarterly report. The correct prediction of the reacting case is very sensitive to the initial roll-up of vortices at the dump plane, as these vortices are only formed if the heat release is delayed somewhat due to the high strain rates in the near-dump shear layer. It will be difficult for steady-state turbulent reacting flow modeling to predict this complex phenomena.

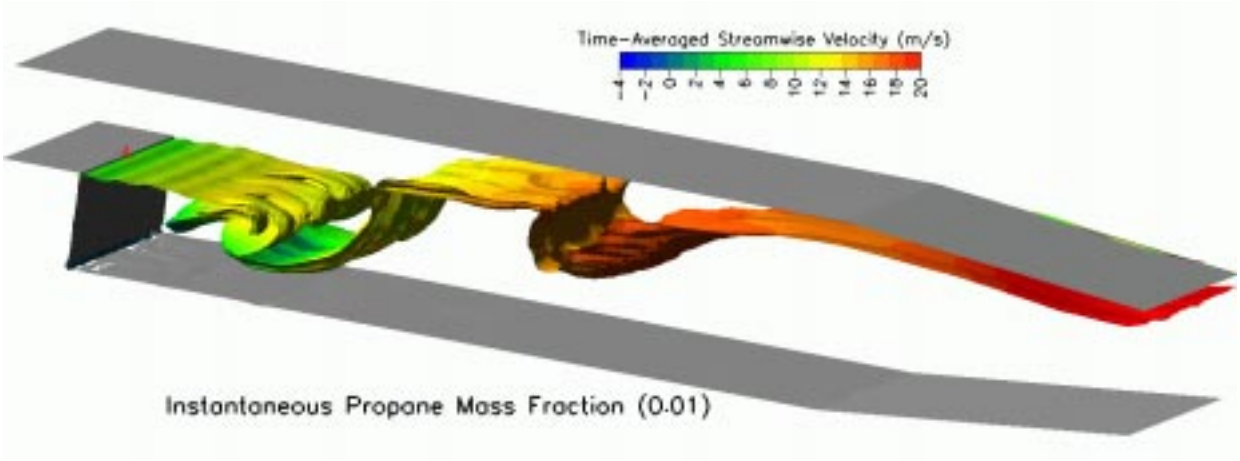

Figure 20. Predicted Snapshot of Propane Mass Fraction (0.01) at 0.0096 Seconds Using LDKM

4.3 Development and Validation of Reduced Chemistry

Several reduced mechanisms have been developed and evaluated for methane-air and hydrogen-air combustion. These mechanisms were developed to give accurate predictions in ignition delay, flame propagation speed, heat release rate, and pollutant formation, such as CO and NO_x. As the reaction rates in current detailed NO_x mechanisms contain large uncertainties, different NO_x mechanisms for rich and lean combustion were examined. For combustion chemistry, either GRI2.11 or GRI3.0 can be used as the base mechanism. Small differences were found in the predicted results for main flame characteristics. Recent experimental data from Dr. Robert Barlow at Sandia National Laboratories in Livermore have suggested that the NO_x mechanism contained in GRI3.0 gives high NO_x levels roughly by a factor of 2 in partially premixed laminar methane-air flames. GRI2.11 gives reasonable results in lean parts of the flame but under-

predicts the NO_x levels in rich parts of the flame. Computed results with a recently modified Miller's mechanism (denoted here as Miller2000) yield much improved NO_x levels for rich parts of the flame where the re-burning process is dominant. Based on the above assessment, Table 1 summarizes the combinations of detailed mechanisms explored during this period for different combustion regimes.

Table 1. Different Combinations of Combustion Chemistry and NO_x Mechanisms

Combustion Chemistry	NO_x Mechanism	Application Regime
GRI2.11	GRI2.11	Lean to stoichiometric
GRI2.11	Miller2000	Rich
GRI3.0	Miller2000	Rich

Calculations were performed for the partially premixed Tsuji flames measured by Barlow and comparisons with the data were made. Figure 21 shows comparisons of measured and predicted NO using the three detailed mechanisms. These results show that the lean side GRI2.1 agrees best with the data. On the rich side, GRI2.1+Miller2000 provided the best agreement with the data. Based on this observation, two 15-step reduced mechanisms with identical species were developed. One from the GRI2.11+Miller2000 and one from GRI2.11. Figures 22 and 23 compare measurements with predictions using the reduced and detailed chemistry. These results show excellent agreement between the reduced and detailed mechanisms.

For hydrogen-air combustion, a subset hydrogen mechanism of GRI2.11 was used as the base mechanism. The NO_x mechanism taken from Miller2000 was then added to the base mechanism. A 7-step reduced chemistry was developed with this combined mechanism and the results are being evaluated. Detailed propane chemistry is currently being obtained from Robert Pitz at Lawrence Livermore. Prof. Chen will then merge the NOx mechanism from Miller and/or GRI2.11 to provide a comprehensive detailed mechanism and then reduce it down to approximately 19 species.

For syngas combustion, the methane mechanism should be appropriate. Since syngas is comprised mainly of CO and H2, and these submechanisms are included in GRI2.11, the reduced mechanism for CH4 will be used.

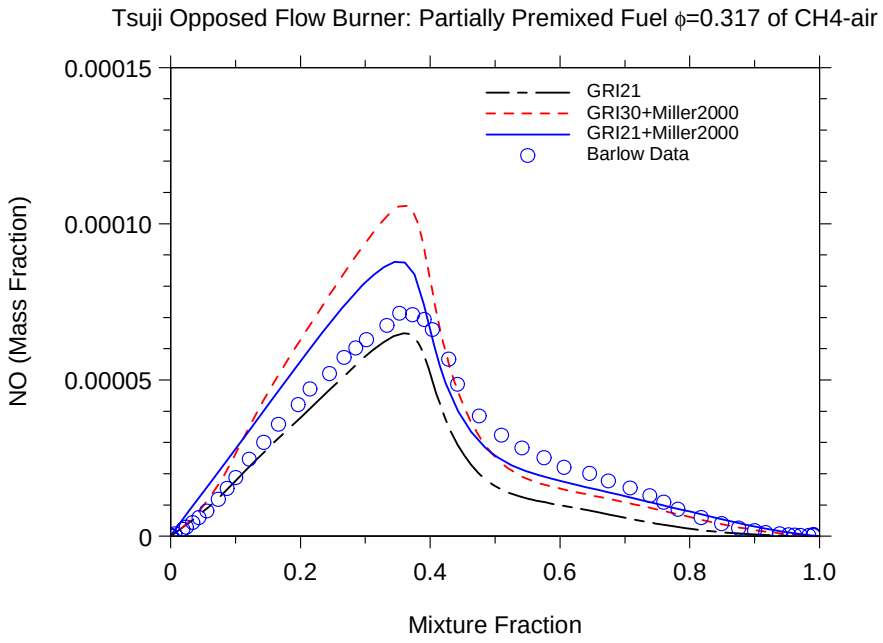

Figure 21. Comparison of Measured and Predicted NO Using Three Detailed Chemical Mechanisms. GTI2.11 provides better agreement on the lean side, while GRI2.11+Miller2000 provides better agreement on the rich side.

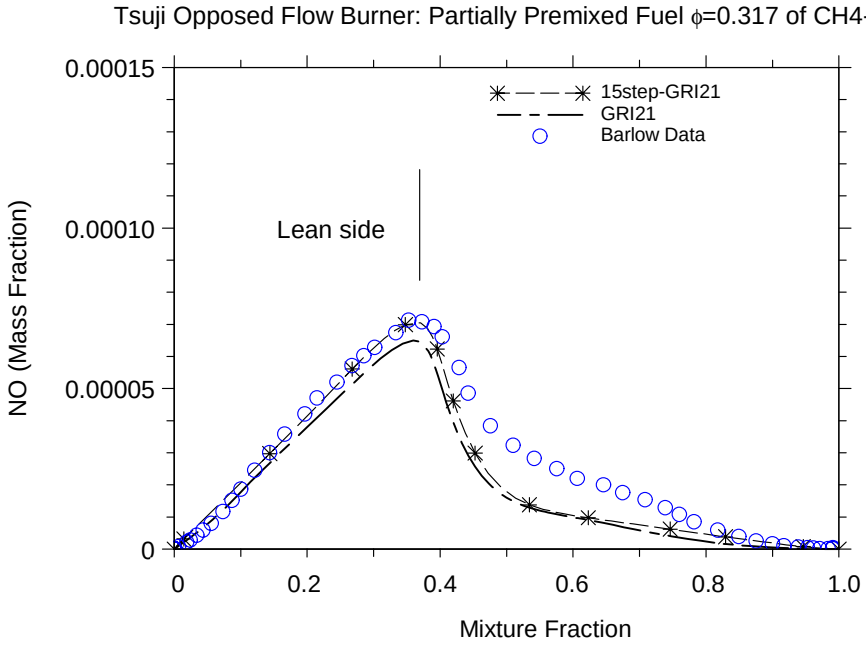

Figure 22. Comparison of Measured and Predicted NO Using GRI2.11 Detailed and 15-step Reduced Chemical Mechanisms. Good agreement is obtained on the lean side.

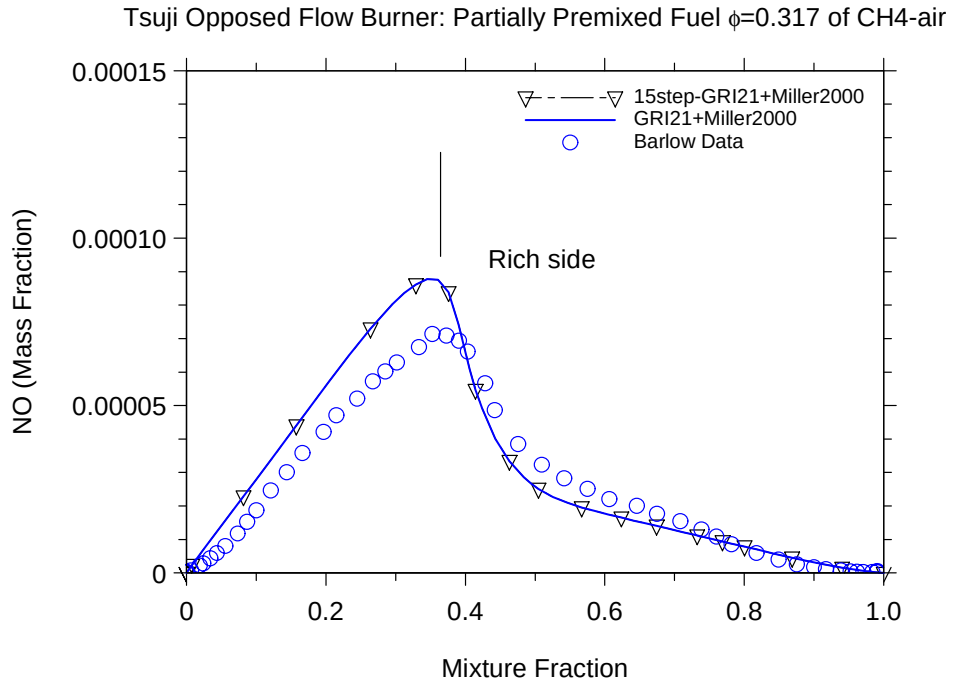

Figure 23. Comparison of Measured and Predicted NO Using GRI2.11+Miller Detailed and 15-step Reduced Chemical Mechanisms. Good agreement is obtained on the rich side.

4.4 Operator Splitting

Within the last quarter, the capability to perform operator splitting was added to CFD-ACE+. This capability allows chemical kinetics to be treated separately from convection and diffusion. The stiff ODE solver DVODE (Brown et al., 1989) was implemented in CFD-ACE+ and advances the species mass fractions due to chemical kinetics for the given time-step. Then, the overall chemical production/consumption rate for each species (Y(t2) –Y(t1))/dt is used as a source term in its governing transport equation. This decoupling of the chemistry from the convection and diffusion provides better convergence of the governing transport equations compared to traditional (sequential) finite volume flow solvers because: (i) the ODE solver was specifically developed to handle stiff chemical kinetics equations (Brown et al., 1989) and (ii) the reaction transport of all species occurs simultaneously, rather than sequentially.

This decoupled chemistry approach is restricted to time-steps that are smaller than the cell residence time, which is easy to achieve when doing LES. The inclusion of subgrid mixing will typically require several reduced timesteps in order to minimize the error due to coupling between small-scale mixing and reaction.

The DVODE solver uses a variable step-size, backward differentiation formula method that requires significant computational effort. In addition to the expense incurred by the ODE solver, significant expense is required to compute chemical reaction rates, particularly if additional iterations must be used to compute steady-state species for a reduced mechanism. Fast table look-up of integrated species increments using Neural Nets and/or In Situ Adaptive Tabulation

(ISAT) will be used to replace the expensive direct integrations required in DVODE. These tabulation algorithms already assume operator splitting, so their implementation will be relatively straightforward.

Detailed testing of the operator splitting technique with multi-step chemistry and these advanced tabulation algorithms will be presented in the next quarterly report. Limited CFD-ACE+ calculations, using operator splitting with a 4-step propane mechanism (Jones and Lindstedt, 1988) and a 15-step steady-state species reduced mechanism for methane (Chen, 2001) have been performed without tabulation.

4.5 In Situ Adaptive Tabulation (ISAT)

The ISAT algorithm is currently being implemented in the LES combustion code. The ISAT algorithm was first conceived by Prof. Pope at Cornell University (Pope, 1997) and has since been coded up by Dr. Virgil Adumitroaie at CFDRC (Leonard and Adumitroaie, 1999). The ISAT algorithm overcomes storage limits with pre-processed look-up tables and computational limits with direct integration. Pre-processed look-up tables are limited to about 5 reactive scalars. The ISAT method, on the other hand, has allowed up to 19 species with a computational speed-up of ~ 100 compared to direct integration (Menon et al., 2000).

Since chemical species evolve through composition space along low-dimensional manifolds, table values are needed for only a fraction of the allowed composition space. In situ tabulation is done as a part of the simulation and when the same composition re-occurs, the binary tree data structure is searched and the stored information is retrieved quickly. The errors arising from the retrieval process are controlled using a procedure based on regions of accuracy. In order to appropriately use a specified region of accuracy, the ODE governing the first order sensitivity coefficients must be computed, along with the chemical species themselves. This sensitivity coefficient ODE requires the Jacobian matrix of the chemical species and is currently being modified in the current ISAT algorithm so that steady-state species mechanisms can be utilized.

4.6 CMC Subgrid Chemistry Model

During the past quarter the Conditional Moment Closure for Large Eddy Simulations has been implemented. The formulation is based on the algorithm developed by Bushe and Steiner (1999), as an alternative to the classical methods for closing the chemical source terms. The algorithm has as a starting point the seminal work by Bilger (1993) and Klimenko (1990) in which a new approach for modeling turbulent reacting flows, called Conditional Moment Closure (CMC) was proposed. The CMC method employs the transport equations of conditionally averaged quantities instead of their spatially filtered counterparts. Variables on which the chemical reactions are known to depend, are chosen to be the conditioning variables. CMC allows the evaluation of the chemical source term in an affordable and sufficiently precise manner.

Furthermore, the methodology applied to LES does not require the solution of the transport equations in the conditioning space. In its present form the proposed model is devised to provide the filtered means of the chemical source terms needed to close the LES set of equations in

reacting flows. This method has proven its predictive capability in an a priori tests using DNS data of a turbulent reacting shear layer.

In non-premixed combustion far from extinction, the reaction rates mainly depend on mixture fraction. Thus, the mixture fraction is clearly an appropriate conditioning variable. In the context of non-premixed combustion, the mixture fraction represents the local fraction of mass originating from the feeding fuel stream. Thus, it is zero in pure oxidizer and one in pure fuel. In the following, the average of some quantity *f*, conditional on the mixture fraction *Z* having some value ζ, will be denoted by an overline

$$\overline{f|Z} = \langle f|Z=\zeta \rangle$$

The conditionally averaged reaction term occurring in the conditionally averaged transport equation for the mass fraction Y_i is closed with the first order CMC hypothesis: the conditional average of the chemical source term of some species *i* can be modeled by evaluating the chemical reaction rates using the conditional averages of the composition vector, temperature, and density. Under the CMC method, the level of perturbations from the modeled mean data is reduced by conditional averaging.

Thus, $\overline{\dot{\omega}_i(Y_k,T,\rho)|Z} = \dot{\omega}_i(\overline{Y_k|Z},\overline{T|Z},\overline{\rho|Z})$.

It has been established that the CMC hypothesis, based on a single conditioning variable, provides adequate predictions of reaction rates for flames far from extinction (Bilger, 1993a; Smith 1994). Furthermore, this method takes advantage of the spatial homogeneity of the conditional averages on particular surfaces in the reacting flow field.

The conditional filtered means are defined using the filtered density function (FDF) denoted by P_L (Pope, 1990):

$$P_L(\psi;\boldsymbol{x},t) = \iiint_{-\infty}^{\infty} G(\boldsymbol{x}'-\boldsymbol{x})\varsigma[\psi,\phi(\boldsymbol{x}',t)]d\boldsymbol{x}'$$

$$\varsigma[\psi;\phi(x',t) = \prod \delta[\psi-\phi(\boldsymbol{x},t)] \equiv \prod_{\alpha=1}^{N_s} \delta[\psi_\alpha - \phi_\alpha(\boldsymbol{x},t)]$$

where δ denotes the delta function and ψ denotes the "composition domain" of the scalar variable. The term is the "fine-grained" density (Pope, 1985). The equation above implies that the FDF is the spatially filtered value of the fine-grained density.

Evaluations of spatial filtered values of the transport variable are achieved by integrating the FDF. In variable density flows, it is useful to define the Favré FDF, $\tilde{P}_L = \overline{\rho P_L}/\overline{\rho}$. Thus, the Favré filtered variable is given by:

$$\tilde{A}(\boldsymbol{x},t) = \int_{-\infty}^{\infty} A(\psi)\tilde{P}_L(\psi;\boldsymbol{x},t)d\psi$$

The density weighted, filtered temperature in each cell can be expressed as

$$\widetilde{T} = \int_0^1 \widetilde{P}_L(Z)\overline{T|Z}dZ$$

where $\overline{T|Z}$ is the ensemble average of the conditional filtered mean temperature for some ensemble *A* of *N* points in the flow. In order to reduce the computational costs the ensemble *A* is composed of the surrounding cell values of the current cell.

The above equation is an integral equation — a Fredholm equation of the first kind — which, for discrete intervals in *Z*, can be inverted to yield the conditional average. Fredholm equations of the first kind are often extremely ill-conditioned. Applying the kernel to a function is generally a smoothing operation, so the solution, which requires inverting the operator, will be extremely sensitive to small changes or errors in the input. Smoothing often actually loses information, and there is no way to get it back in an inverse operation. Specialized methods have been developed for such equations, which are often called inverse problems. In general, a method must augment the information given with some prior knowledge of the nature of the solution. This prior knowledge is then used, in one way or another, to restore lost information.

In the current project we will investigate the effect of the inverse operation algorithm on the performance of the CMC model. Bushe and Steiner (1999) have proposed to approximate simply by numerical quadrature with $M < N$ quadrature points and then obtain the conditional filtered mean in the least square sense. This procedure is valid when the ensemble *A* has a sufficient number of points and can be described as homogeneous. In our case, since we are using this methodology on unstructured grids, we cannot select such an ensemble. Therefore a better inversion method has to be used. We are implementing and will be testing the Richardson-Lucy iterative method used by the image reconstruction community. If necessary, other methods based on the maximum entropy will be considered.

Similar equations can be written for the density and the mass fractions to obtain $\overline{\rho|Z}$ and $\overline{Y_k|Z}$, respectively. Even in the case of non-homogeneity the inversion would still yield an approximation for the conditional average of the temperature on the surface constituted by the ensemble of LES cells. The conditional average of the chemical source terms can now be obtained using the CMC hypothesis.

In this manner, it is possible to obtain closure for the sub-grid scale mean reaction rate for any chemical kinetic mechanism. No assumptions have been made regarding the thickness of the regions in which chemical reactions are significant relative to the turbulent length scales. Only the assumption of statistical homogeneity of the conditional averages of temperature, density, and pressure on some surface must be made. As for the FDF of the mixture fraction, a beta PDF with the same mean and variance can approximate the real FDF appropriately.

In premixed systems, a progress variable is usually defined in terms of a reactive scalar such as temperature. Conditional averages of mass fractions and enthalpy will be taken conditional on

the progress variable, which will be computed from a transport balance equation. All the above modeling considerations regarding the CMC are also valid in the premixed regime.

In order to improve the predictability of the CMC for local extinctions, autoignition and low NOx emissions a second conditioning variable will be utilized. Following the procedure reported by Bushe and Steiner (1999) the second conditioning variable will be taken to be the scalar/progress variable dissipation.

4.7 LEM Subgrid Chemistry Model

Georgia Tech is in the process of setting up the DOE-HAT configuration to evaluate the subgrid LEM model with efficient tabulation (ISAT-ANN) to predict CO and NO emissions. This development work is being performed with Suresh Menon's research LES code. Georgia Tech is still awaiting inflow profiles from P&W, but is exploring issues regarding the grid resolution and the domain needed for a non-reacting flow using the DOE-HAT configuration and flow rate.

The geometry includes an annular inlet dumping into a combustor with a convergent nozzle at the exit. This nozzle is used primarily to ensure that there is no negative flow at the outflow boundary. The impact of this outflow boundary condition on convergence is being explored for a distance of 15 inches downstream of the dump plane (where data is measured and comparison is required). Three domains are being evaluated and include axial lengths of 20, 25 and 35 inches. Figure 24 show a typical grid (approximately 1 million grid points) used to resolve the inlet (which contains a circular insert) and the combustor.

The inlet profiles are currently unavailable, however, P&W is modeling this inlet with a commercial code and will provide these boundary conditions later. Representative profiles have been generated and are shown in Figure 25. The inlet swirl number is approximately 0.9; however at the dump plane it is going to be much less due to readjustment of the flow at the inlet.

At the wall, no slip adiabatic boundary conditions are used. For the inlet and the outlet, we use Poinsot & Lele characteristic inflow and outflow boundary conditions.

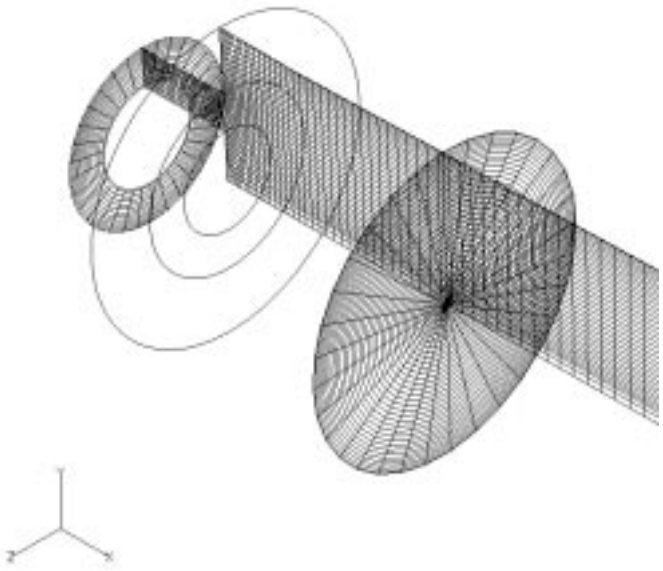

Figure 24. Grid Structure at the Inlet

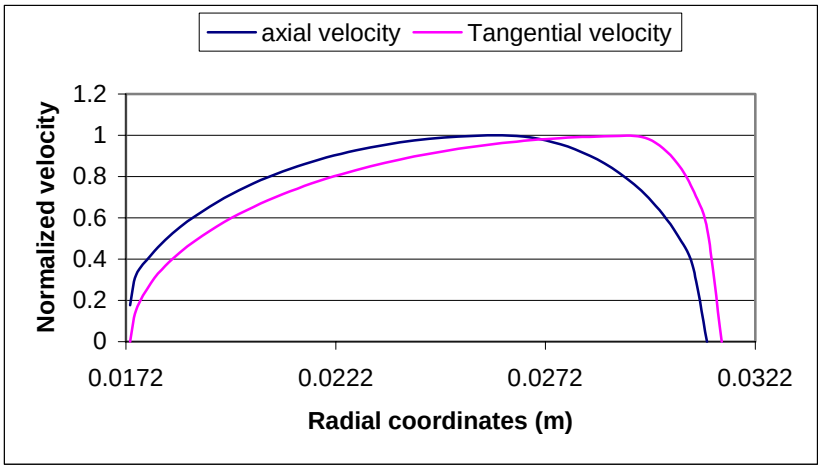

Figure 25. Normalized Velocity Profile Used as Inflow Velocity Conditions

In order to determine the appropriateness of the inflow profiles some non-reacting LES studies in a 9 inch long dump combustor have been carried out. This combustor length is similar to earlier GE LM6000 studies that have been performed at Georgia Tech. The main difference between the earlier case and the present study is that in the DOE-HAT combustor the inlet contains an annular bluff body that will change the fluid dynamics dramatically. A comparison of the earlier LES results (i.e., without the inlet plug) with the present results will be performed.

Figures 26 and 27 show respectively, the vorticity magnitude in the combustor and in the near field of the inlet, and Figure 28 shows the axial velocity contours in the combustor. Both shear layers shedding from the bluff body and the inlet wall are resolved in these simulations. Further analysis of these results are currently underway and will be reported next quarter.

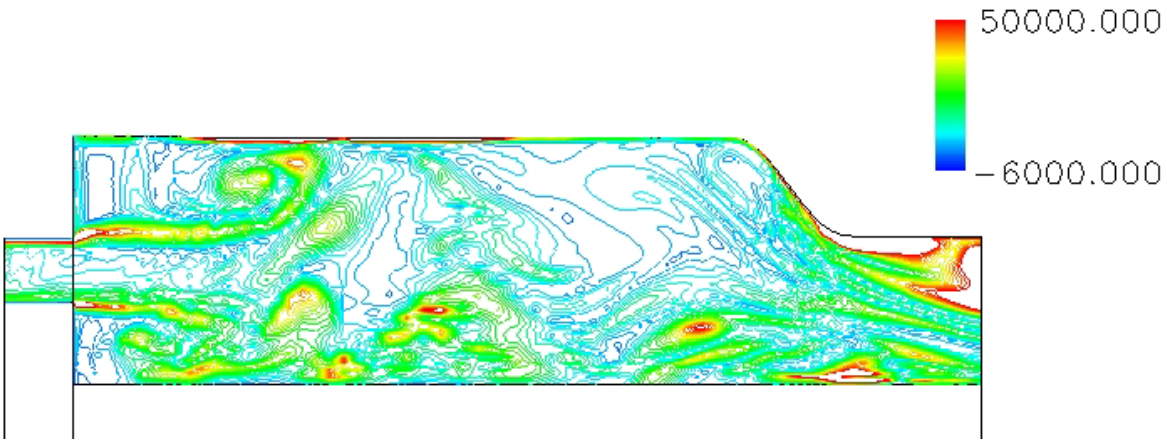

Figure 26. Vorticity Magnitude in the Combustor

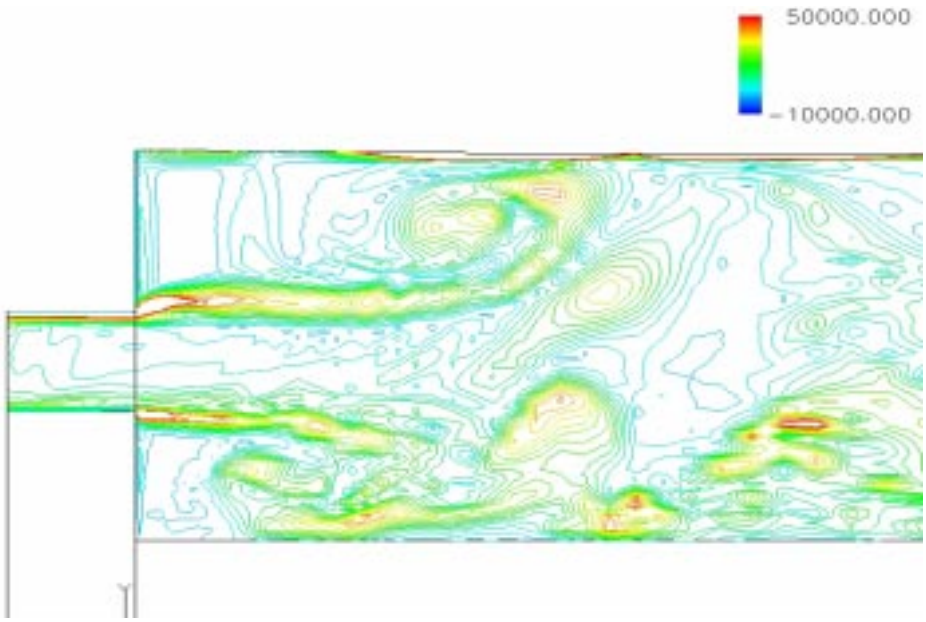

Figure 27. Vorticity Magnitude Neat the Inlet

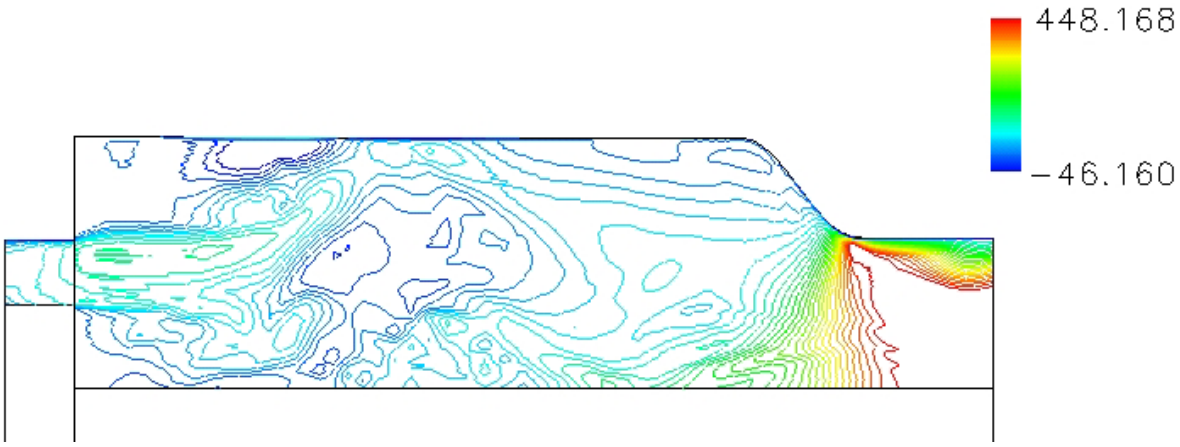

Figure 28. Axial Velocity Contours in the Combustor

A series of cold flow simulations will be used to determine the optimal length needed to ensure that the axial location at 15 inches is not affected by the outflow location. Once that is determined, the grid and the computational domains will be frozen. This effort will be completed within the next month and at the same time studies of full-premixed combustion using the flamelet model will be performed. Experimentally, it was found that the mixing process was not completed before the reactants enter the combustor. In order to make accurate predictions, this unmixedness must be included.

5. CONCLUSION

The combustion LES code has been tested and used successfully to predict combustion and nonreacting turbulent flow dynamics in existing experimental cases. A 2.1 million tetrahedral-cell case, including the details of swirl vanes and fuel spokes, of an unstable DOE-NETL lean premixed combustor was modeled. Excellent oscillating frequencies were predicted, better than previous LES calculations that did not include the fuel injection and swirl details. The localized dynamic subgrid turbulence model allowed for good predictions of reattachment length and velocity profiles in a turbulent flow over a back-step. Finally, reduced chemical models were developed that accurately captured NO_x at rich conditions due to the initial merging of Miller's latest NO_x submechanism with the detailed GRI2.11 mechanism. This chemistry, along with appropriate tabulation and subgrid models, will be implemented in the LES code and tested during the next quarter.

6. REFERENCES

Barlow, R.S., and Frank, J.H., (1998), 27th Symposium (International) on Combustion; The Combustion Institute, Pittsburgh, p. 1087

Bilger, R.W., (1993), "Conditional Moment Closure for Turbulent Reacting Flows," Phys. Fluids A., 5, 436-444.

Brown, P.N., Byrne, G.D., and Hindmarsh, A.C., (1989), "VODE: A Variable Coefficient ODE Solver," *SIAM Journal of Scientific and Statistical Computing,*" Vol. 10, pp. 1038-1051.

Bushe, K. and Steiner, H., (1999), “Conditional Moment Closure for Large Eddy Simulation of Non-premixed Turbulent Reacting Flows,” Phys. Fluids., 11, 1896-1906 .

Cannon, S.M., Adumitroaie, V., and Smith, C.E., (2000), "Combustion Dynamics Modeling Using Parallel, Unstructured-Grid, Large Eddy Simulation", *American Flame Research Committee (AFRC) International Symposium*, Newport Beach, CA, September 2000.

Cannon, S. M., and Smith, C. E., (1998), "Numerical Modeling of Combustion Dynamics In A Lean Premixed Combustor", 1998 International Joint Power Generation Conference, Vol. 1, ASME 1998, Fact-Vol. 22.

Chen, J.-Y. , 2001, Personal communication.

Jones, W.P. and Lindstedt, R.P., (1988), “Global Reaction Schemes for Hydrocarbon Combustion,” *Combustion and Flame*, **73**, 233-249.

Klimenko, A. Yu., (1990), "Multicomponent Diffusion of Various Admixtures in Turbulent Flows," Fluid Dynamics., 25, 327-334

Leonard, A. and Adumitroaie, V., (1998), “An Adaptive Probability Density Function Method for Turbulent Supersonic Combustion Simulations,” SBIR Phase II Final Report, CFDRC Report No. 4426/9.

Menon, S., Kim, W-W., Stone, C., Sekar, B., (1999), “Large-Eddy Simulation of Fuel-Air Mixing and Chemical Reactions in Swirling Flow Combustor,” *30th Plasmadynamic and Lasers Conference*, AIAA 99-3340, Norfolk, VA, June 28 – July 1, 1999.

Pitz, R.W. and Daily, J.W., (1983), "Combustion in a Turbulent Mixing Layer Formed at a Rearward-Facing Step," AIAA J. 21 pp.1565 --1570.

Pope, S.; “Computationally Efficient Implementation of Combustion Chemistry Using In Situ Adaptive Tabulation,” Combustion Theory Modelling, 1, 43-63 (1997).

Richards, G. A., Janus, M.C, (1998), "Characterization of Oscillations, During Premix Gas Turbine Combustion", Journal of Engineering for Gas Turbines and Power, Vol. 120, April 1998.

Sankaran, V., Menon, S., (2000), “Structure of Premixed Turbulent Flames in the Flamelet, Thin-Reaction-Zones and Well-Stirred Reactor Regimes; Submitted to Combustion and Flame,” March 2000.

Weller, H.G., Tabor, G., Gosman, A.D., and Fureby, C., (1998), "Application of a Flame-Wrinkling LES Combustion Model to a Turbulent Mixing Layer," 27th Combustion Symposium (1998).

Xu, J, and Pope, S.B.; “PDF Calculations of Turbulent Nonpremixed Flames with Local Extinction”; Combustion and Flame, 123, 281-307 (2000).

APPENDIX A — WORK SCHEDULE

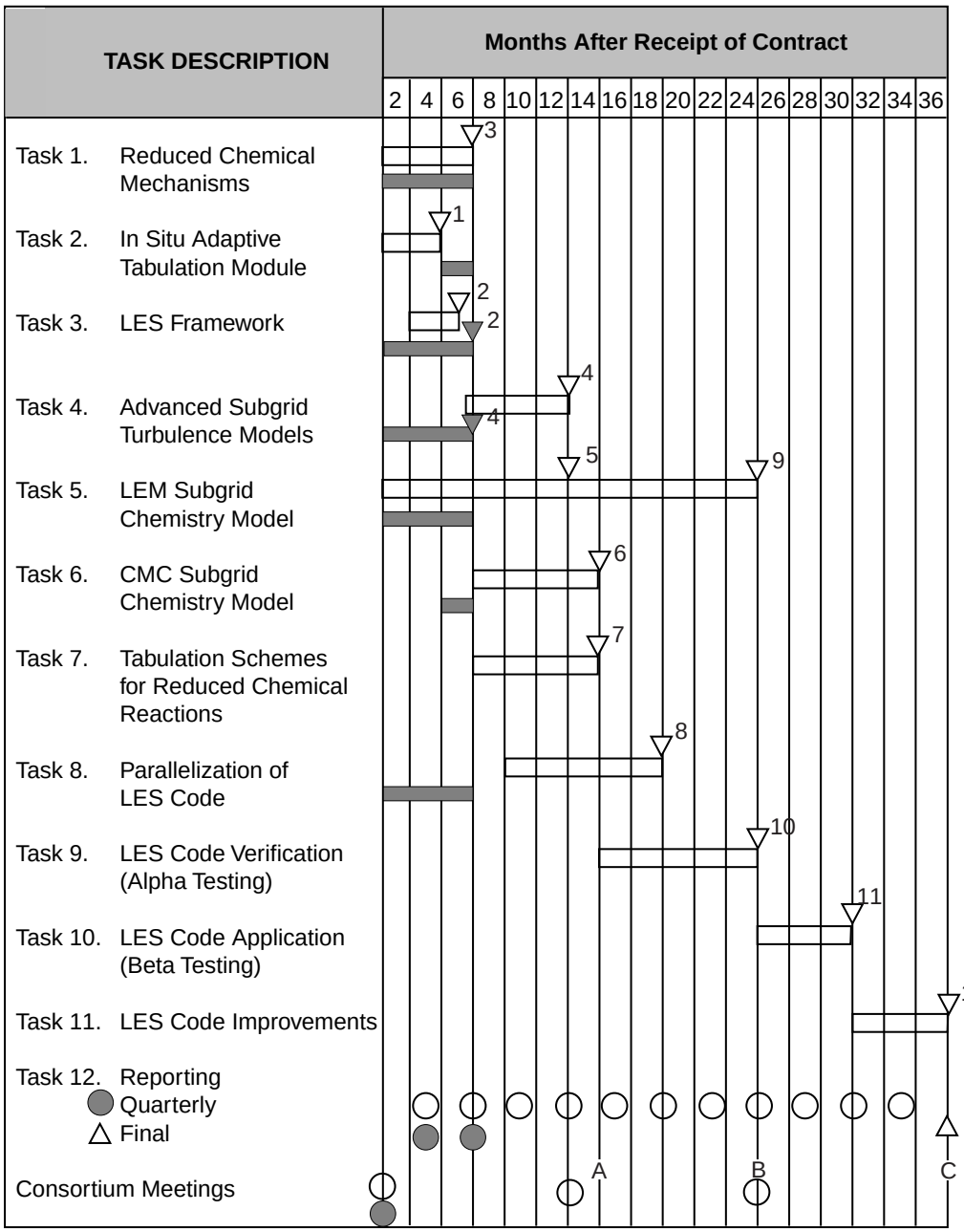

Key Milestones

1 Complete In-Situ Adaptive Tabulation Module
2 Complete LES Framework Modification to CFD-ACE+
3 Complete Reduced Mechanisms
4 Complete Implementation of Turbulence Models
5 Complete Implementation of Initial Version of LEM Model
6 Complete Implementation of CMC Model
7 Complete Tabulation Schemes
8 Complete Parallelization of LES Code
9 Complete Implementation of LEM Model
10 Complete Alpha Testing of LES Code
11 Complete Beta Testing of LES Code
12 Final Release of LES Code

Performance Targets

A Alpha Release of LES Code
B Beta Release of LES Code
C Final Commercial Release of LES Code

Planned
Performed

8321/2

APPENDIX B — FUTURE PLANS

During the next quarter, the following work will be accomplished:

1. Test LES methodology with CMC subgrid model;
2. Develop reduced propane chemical mechanism with NOx emissions;
3. Test LEM/Neural Net model with methane-air data; and
4. Finish development and test ISAT algorithm with reduced chemical mechanisms.